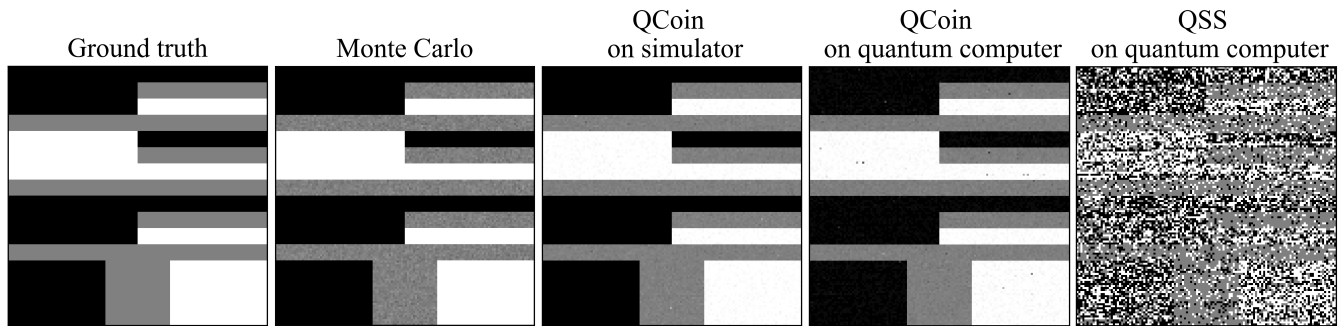


# Quantum Coin Method for Numerical Integration

N. H. Shimada Toshiya Hachisuka

The University of Tokyo



**Figure 1:** Comparison between classical Monte Carlo, quantum supersampling (QSS) [Joh16], and our quantum coin method (QCoin). We used the same 240 queries for each pixel in the numerical experiments, except for QSS on an actual quantum computer which is limited to 7 queries (which is enough to achieve no error for  $f = 0.0, 0.5, 1.0$  on a simulator) due to the limitation of the current architecture of quantum computers. Our QCoin is a quantum variant of classical Monte Carlo, but being a quantum algorithm, QCoin is asymptotically faster than classical Monte Carlo and as efficient as QSS. QCoin, however, is far more robust than QSS on an actual quantum computer.

## Abstract

Light transport simulation in rendering is formulated as a numerical integration problem in each pixel, which is commonly estimated by Monte Carlo integration. Monte Carlo integration approximates an integral of a black-box function by taking the average of many evaluations (i.e., samples) of the function (integrand). For  $N$  queries of the integrand, Monte Carlo integration achieves the estimation error of  $O(1/\sqrt{N})$ . Recently, Johnston [Joh16] introduced quantum supersampling (QSS) into rendering as a numerical integration method that can run on quantum computers. QSS breaks the fundamental limitation of the  $O(1/\sqrt{N})$  convergence rate of Monte Carlo integration and achieves the faster convergence rate. We introduce yet another quantum numerical integration algorithm, quantum coin (QCoin) [AW99], and provide numerical experiments that are unprecedented in the fields of both quantum computing and rendering. We show that QCoin's convergence rate is equivalent to QSS's. We additionally show that QCoin is fundamentally more robust under the presence of noise in actual quantum computers due to its simpler quantum circuit and the use of fewer qubits. Considering various aspects of quantum computers, we discuss how QCoin can be a more practical alternative to QSS if we were to run light transport simulation in quantum computers in the future.

## 1. Introduction

The use of quantum computers for computer graphics is a fascinating idea and potentially leads to a whole new field of research. Lanzagorta and Uhlmann [LU05] mentioned this idea for the first time and suggested many interesting directions for further research. Their primary focus is on Grover's database search algorithm [Gro96], and they showed how its application could lead to fundamentally more efficient algorithms than those on classical computers for various tasks in rendering, such as rasterization, ray casting, and radiosity. Since Lanzagorta and Uhlmann, however, little effort put toward this direction due to the limited availability of actual quantum computers at that time.

Recently, Johnston [Joh16] introduced a quantum algorithm called *Quantum SuperSampling* (QSS) into computer graphics. Johnston proposed to use this algorithm to perform supersampling

of sub-pixels in rendering. This problem is essentially a numerical integration problem in each pixel, which is commonly done by Monte Carlo integration on regular computers. Johnston showed that the performance of this quantum algorithm is fundamentally better than classical Monte Carlo integration in terms of time complexity. On the other hand, his experiments on an actual quantum computer are not as successful as the simulated results due to the presence of noise in quantum computers. Since noise is essentially unavoidable in the current architecture of quantum computers, this issue restricts the use of QSS in practice.

We introduce yet another quantum algorithm for numerical integration which runs well also on *actual* quantum computers; the Quantum Coin method (QCoin). We show that the performance of QCoin is equivalent to QSS both theoretically and numerically, including its convergence rate. We discuss the difference between two

algorithms in terms of their implementations on a quantum computer. Unlike QSS, QCoin can be regarded as a hybrid of quantum-classical algorithm [KMT\*17]. Being a hybrid algorithm, we show how QSS is much more practical than QSS in the presence of noise and the various restrictions on actual quantum computers. We tested our QCoin on a real quantum computer and confirmed that QCoin already shows better performance than classical Monte Carlo integration. We also discuss several open problems for running rendering tasks on quantum computers in the future.

## 2. Background

Before diving into the details of our method, we first summarize some basic concepts of quantum computing for readers who are not familiar with them. While we do cover the basics that are necessary to understand our method in this paper, for some further details, readers might want to refer to a textbook [NC11].

**Single-qubit and superposition.** On a classical computer, all the information is stored as a set of *bits* where each bit represents only one of the two discrete states; e.g., up or down spin on a magnetic storage device, representing a binary number 0 or 1. On a quantum computer, however, a single *qubit* can represent a *superposition* of both 0 and 1 as

$$|\psi\rangle = a|0\rangle + \sqrt{1-a^2}|1\rangle \quad (1)$$

where  $a \in [-1, 1]$  is called an *amplitude* of the state  $|0\rangle$ . While an amplitude is generally a complex number, for simplicity, we focus on cases where it is a real number in this paper.

Unlike the classical case, the states  $|0\rangle$  and  $|1\rangle$  in Equation 1 are *probabilistic*. As such, the same  $|\psi\rangle$  would still give us a different result every time we *measure*  $|\psi\rangle$ . To be precise, the measurement of  $|\psi\rangle$  returns  $|0\rangle$  with the probability  $a^2$  and  $|1\rangle$  with the probability  $1-a^2$ . A classical bit is equivalent to the case of  $|a|^2 = 0$  or 1, and it can be considered as a special case of a qubit.

**Quantum logic gates.** Just like logic gates for bits on classical computers, there are several known *quantum logic gates* that are used to manipulate qubits. We summarize some of them here.

Identity gate  $\hat{I}$

$$\begin{aligned} \hat{I}|0\rangle &= |0\rangle \\ \hat{I}|1\rangle &= |1\rangle \end{aligned}$$

Hadamard gate  $\hat{H}$

$$\begin{aligned} \hat{H}|0\rangle &= \frac{|0\rangle + |1\rangle}{\sqrt{2}} \\ \hat{H}|1\rangle &= \frac{|0\rangle - |1\rangle}{\sqrt{2}} \end{aligned}$$

Pauli  $\hat{X}, \hat{Z}$  gates

$$\begin{aligned} \hat{X}|0\rangle &= |1\rangle, & \hat{Z}|0\rangle &= |0\rangle \\ \hat{X}|1\rangle &= |0\rangle, & \hat{Z}|1\rangle &= -|1\rangle \end{aligned}$$

Rotation gate  $U_\theta$

$$\begin{aligned} U_\theta|0\rangle &= \cos\theta|0\rangle + \sin\theta|1\rangle \\ U_\theta|1\rangle &= -\sin\theta|0\rangle + \cos\theta|1\rangle \end{aligned}$$

( $\theta$  is a rotation angle in the plane spanned by  $|0\rangle$  and  $|1\rangle$ )

**Multi-qubits.** We express a multi-qubit state by concatenating single-qubit states. For example, a two-qubits state whose qubits are both  $|0\rangle$  is expressed as  $|0\rangle \otimes |0\rangle$  or  $|00\rangle$ . The symbol  $\otimes$  represents a tensor product which means the concatenation of qubits in this case. In the following, we omit the symbol  $\otimes$  for simplicity when it is obvious. In general, a two-qubits state whose qubits are both superposition states as Equation 1 can be written as

$$\begin{aligned} |\psi\rangle_a &= a_0|0\rangle + a_1|1\rangle, \\ |\psi\rangle_b &= b_0|0\rangle + b_1|1\rangle \\ \rightarrow |\psi\rangle_a \otimes |\psi\rangle_b &= (a_0|0\rangle + a_1|1\rangle) \otimes (b_0|0\rangle + b_1|1\rangle) \\ &= a_0b_0|00\rangle + a_0b_1|01\rangle + a_1b_0|10\rangle + a_1b_1|11\rangle. \end{aligned}$$

Since this explicit binary notation quickly becomes tedious for many qubits, we use another notation  $|i\rangle$  for a decimal number  $i$  in the binary representation  $i_{n-1} \dots i_1 i_0$  as

$$|i\rangle \equiv |i_{n-1}\rangle \otimes \dots \otimes |i_1\rangle \otimes |i_0\rangle. \quad (2)$$

For example, in the case of 4 qubits, we write as  $|0\rangle = |0000\rangle$ ,  $|1\rangle = |0001\rangle$ ,  $|2\rangle = |0010\rangle$ ,  $\dots$ ,  $|15\rangle = |1111\rangle$ .

**Quantum operation as a tensor product.** In quantum computing, tensor products are also used to represent logic gate operations. For example, given the initial two-qubits state  $|0\rangle \otimes |0\rangle$ , the application of the Hadamard  $\hat{H}$  gate for the first qubit and the Pauli  $\hat{Z}$  gate for the second qubit can be written as

$$(\hat{H} \otimes \hat{Z})(|0\rangle \otimes |0\rangle) = \hat{H}|0\rangle \otimes \hat{Z}|0\rangle. \quad (3)$$

If we only operate the  $\hat{H}$  gate for the first qubit and leave the second qubit unchanged, we can use the identity gate  $\hat{I}$ :

$$(\hat{H} \otimes \hat{I})|0\rangle \otimes |0\rangle. \quad (4)$$

When we apply the same gate to all the qubits, we omit the  $\otimes$  symbol and simplify the notation as

$$\hat{H}|00\rangle \equiv \hat{H}|0\rangle \otimes \hat{H}|0\rangle. \quad (5)$$

This notation is also adopted in the case of the decimal representation in Equation 2. For instance, the operation of the  $\hat{H}$  gate to the 4 qubits  $|0\rangle$  state is written as

$$\begin{aligned} \hat{H}|0\rangle &\equiv \hat{H}|0000\rangle = \hat{H}|0\rangle \otimes \hat{H}|0\rangle \otimes \hat{H}|0\rangle \otimes \hat{H}|0\rangle \\ &= \frac{|0\rangle + |1\rangle}{\sqrt{2}} \otimes \frac{|0\rangle + |1\rangle}{\sqrt{2}} \otimes \frac{|0\rangle + |1\rangle}{\sqrt{2}} \otimes \frac{|0\rangle + |1\rangle}{\sqrt{2}} \\ &= \frac{1}{\sqrt{2^4}} (|0000\rangle + |0001\rangle + \dots + |1111\rangle) = \frac{1}{\sqrt{2^4}} \sum_{i=0}^{15} |i\rangle. \quad (6) \end{aligned}$$

Note that  $\hat{H}|0\rangle$  results in a superposition of all the  $|i\rangle$  states which is often used in quantum algorithms.



a target quantum state by amplifying its amplitude and thus its observation probability. We consider an oracle  $\hat{O}$  which results in

$$|\psi\rangle = \hat{O}|00\dots 0\rangle = \cos\theta|\alpha\rangle + \sin\theta|\beta\rangle \quad (11)$$

where  $|\beta\rangle$  is a target state and  $|\alpha\rangle$  is the other state. The state  $|\psi\rangle$  is represented as a vector  $(\cos\theta, \sin\theta)$  within a plane spanned by  $|\alpha\rangle$  and  $|\beta\rangle$  as shown in Figure 2. The goal is to increase the probability of observing the target state, as much as possible. The idea is to rotate  $|\psi\rangle$  counter-clockwise (i.e., making  $\theta$  larger). Figure 2 illustrates this idea.

In AA, we first apply a flip operation  $\hat{R}_f$  which flips the state  $|\psi\rangle$  against the  $|\alpha\rangle$  vector. It can be realized by flipping the sign of target states as  $|\beta\rangle \rightarrow -|\beta\rangle$ . We then project the resulting flipped state  $\hat{R}_f|\psi\rangle$  onto the original  $|\psi\rangle$ , and multiply the length of the projected vector  $|\psi\rangle \langle\psi|\hat{R}_f|\psi\rangle$  by two. Finally, we subtract  $\hat{R}_f|\psi\rangle$  from it. The resulting state

$$|\psi_{\text{result}}\rangle = \cos 3\theta|\alpha\rangle + \sin 3\theta|\beta\rangle \quad (12)$$

has a larger amplitude for  $|\beta\rangle$  than the initial state  $|\psi\rangle$ . The overall operation  $\hat{G}$  is defined as

$$\begin{aligned} |\psi_{\text{result}}\rangle = \hat{G}|\psi\rangle &\equiv (2|\psi\rangle\langle\psi| - \hat{I})\hat{R}_f|\psi\rangle - \hat{R}_f|\psi\rangle \\ &= (2|\psi\rangle\langle\psi| - \hat{I})\hat{R}_f|\psi\rangle \end{aligned} \quad (13)$$

$$\begin{aligned} &= (2\hat{O}|00\dots 0\rangle\langle 00\dots 0| - \hat{I})\hat{R}_f|\psi\rangle \\ &= \hat{O}(2|00\dots 0\rangle\langle 00\dots 0| - \hat{I})\hat{O}^{-1}\hat{R}_f|\psi\rangle. \end{aligned} \quad (14)$$

The  $(2|00\dots 0\rangle\langle 00\dots 0| - \hat{I})$  operation corresponds to flipping the amplitude of all the states except the state  $|00\dots 0\rangle$ . Since  $\hat{G}$  includes two oracle gates ( $\hat{O}$  and  $\hat{O}^{-1}$ ), the AA algorithm makes two queries (i.e.,  $\hat{O}$  is called two times) to perform one  $\hat{G}$  operator. Note that AA does not need to know the actual value of  $\theta$ .

### 3.2. Quantum Fourier Transformation

Quantum Fourier transformation (QFT) can be thought as an analogy to classical discrete Fourier transformation, but on a quantum computer. Given a data set  $\{a_0, a_1, a_2, \dots, a_{N-1}\}$ , classical Fourier transformation  $\{a_k | 0 \leq k \leq N-1\} \rightarrow \{b_j | 0 \leq j \leq N-1\}$  conducts the calculation as  $b_j = \frac{1}{\sqrt{N}} \sum_{k=0}^{N-1} e^{-i\frac{2\pi}{N}jk} a_k$ . The resulting set  $\{b_j\}$  is a set of frequency components of the input data series  $\{a_i\}$ , and one can view that Fourier transform is an algorithm which converts  $\{a_i\}$  into  $\{b_j\}$ .

In QFT, the input data series is given by the amplitudes:

$$|\psi\rangle = a_0|0\rangle + a_1|1\rangle + \dots + a_{N-1}|N-1\rangle. \quad (15)$$

The idea of QFT is to turn this input quantum state into a superposition of frequency components  $\{b_j\}$  as

$$|\psi_{\text{QFT}}\rangle = b_0|0\rangle + b_1|1\rangle + \dots + b_{N-1}|N-1\rangle. \quad (16)$$

We will not explain the detailed process of QFT in this paper as it is not important for our discussion. Interested readers can refer to a textbook of quantum computing [NC11]. The important difference from the classical algorithm is that we cannot directly access frequency components  $b_j$ . Instead, it is only that the observation probability of each state is proportional to  $b_j^2$ .

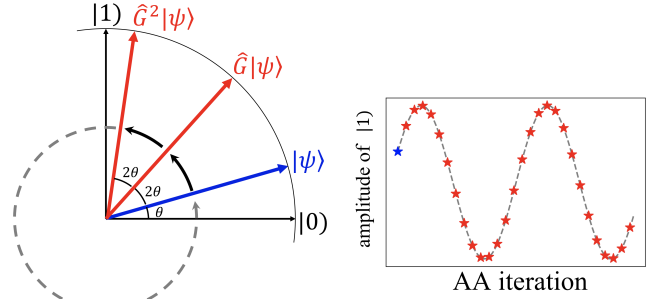


**Figure 3:** Example of repeated AA operations.  $\theta$  is initially defined as  $f = \sin\theta$ . The degree of state vector evolves as  $\theta \rightarrow 3\theta \rightarrow 5\theta \dots$  (left). Therefore, the trace of  $f$  values tracks a sin curve (right).

### 3.3. Quantum Supersampling

Grover [Gro98] was the first to introduce a quantum algorithm for estimating a mean  $f = \frac{1}{M} \sum_{i=1}^M F(i)$ . The idea is to combine AA with QFT as we explain later. Many theoretical developments have followed since then [BHT06, BdSGT11], but few numerical experiments using simulation have been done so far [TKI99].

Johnston [Joh16] implemented this original idea by Grover to conduct numerical experiments in the context of rendering. The problem addressed there is supersampling of an image, which can be seen as a mean estimation per pixel. We explain QSS by Johnston in the following, to contrast it to our QCoin. In the original work by Johnston [Joh16], the values of  $F(i)$  are assumed to be binary  $\{0, 1\}$ . We slightly modified the original algorithm to be able to handle continuous values of  $F(i)$ . Since the algorithms essentially stay the same even with this modification, we refer to our modified QSS simply as QSS in the following.

**Main idea.** The main idea of QSS is to exploit the existence of a periodic cycle when we keep applying amplitude amplification on  $|\psi\rangle$ . As we explained before, AA rotates the state within the plane spanned by  $|\alpha\rangle$  and  $|\beta\rangle$ ; thus the state actually rotates fully after sufficiently many AA operations. It turns out that there is a unique periodic cycle to each corresponding  $\theta$  value. Figure 3 shows the movement of the state vector  $|\psi\rangle$  (left) and the trace of the amplitude value of  $|1\rangle$  (right). Applying QFT on the history of rotated  $|\psi\rangle$ , we can extract the frequency of this periodic cycle, which then allows us to calculate the corresponding  $\theta$  (and therefore  $f$ ).

**Problem setting.** In QSS, given a black-box function  $F(a) : a \rightarrow [0, 1]$  and a quantum oracle operator

$$\hat{Q}_F : |0\rangle \otimes |i\rangle \rightarrow \left( \sqrt{1-F(i)}|0\rangle + \sqrt{F(i)}|1\rangle \right) \otimes |i\rangle, \quad (17)$$

the objective is to get the average  $f$  of  $F(a)$  with  $N(=2^n)$  samples:

$$f \equiv \frac{1}{N} \sum_{i=0}^{N-1} F(i). \quad (18)$$

**Algorithm.** In QSS, we use the oracle  $\hat{Q}_F$  and make a superposition state  $|\psi_0\rangle$  from the initial state whose all qubits (= register, target, and input qubits) are  $|0\rangle$ , where the numbers of qubits for each are  $\log_2 P$ , 1,  $\log_2 N$ . We thus write the initial state as

$$\underbrace{|0\dots 0\rangle}_{\log_2 P} \otimes |0\rangle \otimes \underbrace{|0\dots 0\rangle}_{\log_2 N} = |0\rangle \otimes |0\rangle \otimes |0\rangle \quad (19)$$

The superposition state  $|\psi_0\rangle$  is derived as follows:

$$|\psi_0\rangle = \hat{Q}_F(\hat{H} \otimes \hat{I} \otimes \hat{H})|0\rangle \otimes |0\rangle \otimes |0\rangle \quad (20)$$

$$= \frac{1}{\sqrt{PN}} \sum_{m=0}^{P-1} \sum_{i=0}^{N-1} |m\rangle \otimes \hat{Q}_F(|0\rangle \otimes |i\rangle) \quad (21)$$

$$= \frac{1}{\sqrt{PN}} \sum_{m=0}^{P-1} \sum_{i=0}^{N-1} |m\rangle \otimes \left( \sqrt{1-F(i)}|0\rangle + \sqrt{F(i)}|1\rangle \right) \otimes |i\rangle \quad (22)$$

The total measurement probability of  $\frac{1}{\sqrt{N}} \sum_{i=0}^{N-1} \sqrt{F(i)}|1\rangle \otimes |i\rangle$  states is  $\sum_{i=0}^{N-1} \sqrt{\frac{F(i)}{N}} = f$ . If we define  $|0\rangle' \equiv \frac{1}{\sqrt{N}} \sum_{i=0}^{N-1} |0\rangle \otimes |i\rangle$  and  $|1\rangle'$  in the same manner, the amplitude of  $|1\rangle'$  is  $\sqrt{f}$ :

$$|\psi_0\rangle = \frac{1}{\sqrt{P}} \sum_{m=0}^{P-1} |m\rangle \otimes \left( \sqrt{1-f}|0\rangle' + \sqrt{f}|1\rangle' \right).$$

We can define  $\cos\theta$  and  $\sin\theta$  as  $\sqrt{1-f}$  and  $\sqrt{f}$ , and  $|\psi_0\rangle$  is

$$|\psi_0\rangle = \frac{1}{\sqrt{P}} \sum_{m=0}^{P-1} |m\rangle \otimes (\cos\theta|0\rangle' + \sin\theta|1\rangle'). \quad (23)$$

We then apply AA to the  $(\cos\theta|0\rangle' + \sin\theta|1\rangle')$  state for  $P$  times all the register qubits to obtain their superposition  $|\psi_1\rangle$

$$|\psi_1\rangle = \frac{1}{\sqrt{P}} \sum_{m=0}^{P-1} |m\rangle (\cos(2m+1)\theta|0\rangle' + \sin(2m+1)\theta|1\rangle'). \quad (24)$$

We then measure the target state. We assume that the state is converged to  $|1\rangle'$ :

$$|\psi_2\rangle = \frac{1}{C} \sum_{m=0}^{P-1} \sin(2m+1)\theta |m\rangle |1\rangle' \quad (25)$$

Finally, we perform QFT on  $|\psi_2\rangle$ . With a sufficiently large probability [BHT06], the result of measurement after QFT will be

$$t \simeq \frac{P\theta}{\pi}, \frac{P(\pi-\theta)}{\pi}. \quad (26)$$

If the measured and converged state is  $|0\rangle'$ , we get the same result. Therefore, we can deduce the estimated average  $f'$  by

$$f \approx f' = \sin^2\left(\frac{t\pi}{P}\right) \quad (27)$$

Since  $\frac{t\pi}{P}$  can be determined by the precision  $O(1/P)$  in this process,  $f'$  also has the precision of  $O(1/P)$ . Johnston [Joh16] proposed to use a precomputed table instead of the analytical expression in Equation 27 by considering only discrete values of  $f$ . The estimation error  $|f - f'|$  is inversely proportional to the number of AA operations  $P$ . Since AA uses two queries per operation, we perform  $O(N)$  queries to achieve  $O(1/N)$  error. Note that this convergence rate is faster than  $O(1/\sqrt{N})$  of Monte Carlo integration.

**Example.** We show how the whole process works for the 5 qubits case where  $P = 4$  and  $N = 4$ . The initial state of 5 qubits is  $(|0\rangle \otimes |0\rangle) \otimes |0\rangle \otimes (|0\rangle \otimes |0\rangle) = |0\rangle \otimes |0\rangle \otimes |0\rangle$ . At first, we apply  $\hat{H} \otimes \hat{I} \otimes \hat{H}$  as in Equation 20:

$$\begin{aligned} & (\hat{H} \otimes \hat{I} \otimes \hat{H}) |0\rangle \otimes |0\rangle \otimes |0\rangle \\ &= \left( \frac{|0\rangle + |1\rangle + |2\rangle + |3\rangle}{\sqrt{4}} \right) \otimes |0\rangle \otimes \left( \frac{|0\rangle + |1\rangle + |2\rangle + |3\rangle}{\sqrt{4}} \right). \end{aligned}$$

This transformation is as Equation 6. Then, the oracle  $\hat{Q}_F$  works as

$$\begin{aligned} & \hat{Q}_F |0\rangle \otimes \left( \frac{|0\rangle + |1\rangle + |2\rangle + |3\rangle}{\sqrt{4}} \right) \\ &= \frac{1}{\sqrt{4}} \left( \sqrt{1-F(0)}|0\rangle + \sqrt{F(0)}|1\rangle \right) \otimes |0\rangle \\ &+ \frac{1}{\sqrt{4}} \left( \sqrt{1-F(1)}|0\rangle + \sqrt{F(1)}|1\rangle \right) \otimes |1\rangle \\ &+ \frac{1}{\sqrt{4}} \left( \sqrt{1-F(2)}|0\rangle + \sqrt{F(2)}|1\rangle \right) \otimes |2\rangle \\ &+ \frac{1}{\sqrt{4}} \left( \sqrt{1-F(3)}|0\rangle + \sqrt{F(3)}|1\rangle \right) \otimes |3\rangle. \end{aligned}$$

Since  $\hat{Q}_F$  does not operate on the 1st register qubits, we omitted it above. The probability of observing  $|1\rangle$  is calculated as

$$\left| \sqrt{\frac{F(0)}{4}} \right|^2 + \left| \sqrt{\frac{F(1)}{4}} \right|^2 + \left| \sqrt{\frac{F(2)}{4}} \right|^2 + \left| \sqrt{\frac{F(3)}{4}} \right|^2 = f$$

hence the total amplitude of  $|1\rangle$  is  $\sqrt{f}$ . By grouping a set of states with  $|1\rangle$  as  $|1\rangle'$  (and those with  $|0\rangle$  as  $|0\rangle'$ ) for brevity, the resulting state vector can be written as  $\sqrt{1-f}|0\rangle' + \sqrt{f}|1\rangle' = \cos\theta|0\rangle' + \sin\theta|1\rangle'$  where we write  $\sqrt{f} = \sin\theta$ . The state  $|\psi_0\rangle$  is

$$|\psi_0\rangle = \left( \frac{|0\rangle + |1\rangle + |2\rangle + |3\rangle}{\sqrt{4}} \right) \otimes \cos\theta|0\rangle' + \sin\theta|1\rangle'.$$

We perform AA operations ( $\hat{G}$ ) corresponding to the decimal number of the register qubits' state

$$\begin{aligned} |\psi_1\rangle &= \frac{1}{\sqrt{4}} |0\rangle \otimes \hat{G}^0 (\cos\theta|0\rangle' + \sin\theta|1\rangle') \\ &+ \frac{1}{\sqrt{4}} |1\rangle \otimes \hat{G}^1 (\cos\theta|0\rangle' + \sin\theta|1\rangle') \\ &+ \frac{1}{\sqrt{4}} |2\rangle \otimes \hat{G}^2 (\cos\theta|0\rangle' + \sin\theta|1\rangle') \\ &+ \frac{1}{\sqrt{4}} |3\rangle \otimes \hat{G}^3 (\cos\theta|0\rangle' + \sin\theta|1\rangle') \\ &= \frac{1}{\sqrt{4}} |0\rangle \otimes (\cos\theta|0\rangle' + \sin\theta|1\rangle') \\ &+ \frac{1}{\sqrt{4}} |1\rangle \otimes (\cos 3\theta|0\rangle' + \sin 3\theta|1\rangle') \\ &+ \frac{1}{\sqrt{4}} |2\rangle \otimes (\cos 5\theta|0\rangle' + \sin 5\theta|1\rangle') \\ &+ \frac{1}{\sqrt{4}} |3\rangle \otimes (\cos 7\theta|0\rangle' + \sin 7\theta|1\rangle'). \end{aligned}$$

We then measure the target qubit  $|1\rangle'$  to obtain  $|\psi_2\rangle = \frac{1}{C} (\sin\theta|0\rangle + \sin 3\theta|1\rangle + \sin 5\theta|2\rangle + \sin 7\theta|3\rangle) \otimes |1\rangle'$  which allows us to estimate  $\theta$  (thus  $f$ ) value using QFT.



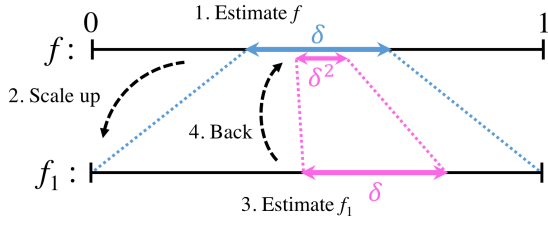


**Figure 4:** Shifting-Scaling process of QCoin: 1. We estimate the value of  $f$  and decide bounded-error range:  $[f' - \frac{\delta}{2}, f' + \frac{\delta}{2}]$ . 2. We scale up quantum coin to  $[0, 1]$ . 3. Now the target value  $f$  is changed to  $f_1$ , we can estimate  $f_1$  with  $\delta$  error. 4. We can estimate  $f$  with  $\delta^2$  error via calculating back from estimated  $f_1$  value.

#### 4. Quantum Coin Method

We introduce another mean-estimation quantum algorithm, which we call as the *quantum coin method* (QCoin). While the theory of QCoin was introduced by Abrams and Williams 20 years ago [AW99], its actual implementation was not discussed, and no numerical experiment has been done so far. We provide the first practical implementation of this algorithm by identifying practical issues and performed the first set of numerical experiments.

**Quantum coin.** QCoin uses a *quantum coin* as its core. It is constructed with an oracle gate as a quantum state including a target state  $|1\rangle$  with the observation probability equal to  $f^2$  as in Equation 10. Measurement of this state returns the target state  $|1\rangle$  ("head") with the probability of  $f^2$ , and other states  $|0\rangle$  ("tail") with the probability  $1 - f^2$ . By counting the number of "heads" out of the total number of trials, we can estimate  $f^2$  (and  $f$ ) with  $\delta$  error with  $O(1/\delta^2)$  queries. As we discussed before, this process alone is equivalent to Monte Carlo integration, thus it will not provide any benefit.

**Main idea.** Suppose that we have a rough estimate  $f'$  by running Monte Carlo integration using a quantum coin as described above with  $N$  queries. According to the error analysis of Monte Carlo integration, with a certain confidence probability, one can say that the actual value of  $f$  is in the interval of  $[f' - \frac{\delta}{2}, f' + \frac{\delta}{2}]$  where  $\delta = O(1/\sqrt{N})$ . The idea of QCoin is to repeatedly shrink this interval by shifting and scaling it using quantum computation until we are sufficiently close to  $f$ . Figure 4 illustrates this process.

**Problem setting.** QCoin considers a black-box function

$$F(a) : a \rightarrow [0, 1] \quad (28)$$

and a quantum oracle operator  $\hat{Q}_{F,E}$  which includes the function  $F(a)$  and the offset (shifting) parameter  $E$ :

$$\hat{Q}_{F,E} |0\rangle \otimes |i\rangle \rightarrow \left( \sqrt{1 - (F(i) - E)^2} |0\rangle + (F(i) - E) |1\rangle \right) \otimes |i\rangle. \quad (29)$$

Our goal is to estimate the average value  $f$  similar to QSS.

**Algorithm.** For the first step, using oracle  $\hat{Q}_{F,0}$ , we make the initial superposition state:

$$\begin{aligned} |\psi_0\rangle &= \hat{Q}_{F,0} (\hat{I} \otimes \hat{H}) |0\rangle \otimes |0\rangle \\ &= \hat{Q}_{F,0} \sum_{i=0}^{N-1} |0\rangle \otimes |i\rangle \\ &= \frac{1}{\sqrt{N}} \sum_{i=0}^{N-1} \left( \sqrt{1 - F(i)^2} |0\rangle + F(i) |1\rangle \right) \otimes |i\rangle \quad (30) \end{aligned}$$

The construction of a quantum coin is in fact simple; we perform  $\hat{H}$  operators for all the qubits after the oracle gate operation. After this process, each state is distributed with  $\frac{1}{\sqrt{N}}$  amplitude to a  $|0\rangle$  state and any amplitude to all the other states:

$$\begin{aligned} |\psi_0\rangle' &= (\hat{I} \otimes \hat{H}) |\psi_0\rangle \\ &= \frac{1}{N} \sum_{i=0}^{N-1} F(i) |1\rangle \otimes |0\rangle + \dots = f |1\rangle \otimes |0\rangle + \dots \quad (31) \end{aligned}$$

We show the construction of a quantum coin for the 3 qubits case. The initial state of 3 qubits is  $|0\rangle \otimes (|0\rangle \otimes |0\rangle) = |0\rangle \otimes |0\rangle$ . Applying  $\hat{I} \otimes \hat{H}$  operation, we have

$$(\hat{I} \otimes \hat{H}) (|0\rangle \otimes |0\rangle) = |0\rangle \otimes \left( \frac{|0\rangle + |1\rangle + |2\rangle + |3\rangle}{\sqrt{4}} \right).$$

We get  $|\psi_0\rangle$  in Equation 30 using  $\hat{Q}_{F,0}$ :

$$\begin{aligned} |\psi_0\rangle &= \hat{Q}_{F,0} |0\rangle \otimes \left( \frac{|0\rangle + |1\rangle + |2\rangle + |3\rangle}{\sqrt{4}} \right) \\ &= \frac{1}{\sqrt{4}} \left( \sqrt{1 - F(0)^2} |0\rangle + F(0) |1\rangle \right) \otimes |0\rangle \\ &\quad + \frac{1}{\sqrt{4}} \left( \sqrt{1 - F(1)^2} |0\rangle + F(1) |1\rangle \right) \otimes |1\rangle \\ &\quad + \frac{1}{\sqrt{4}} \left( \sqrt{1 - F(2)^2} |0\rangle + F(2) |1\rangle \right) \otimes |2\rangle \\ &\quad + \frac{1}{\sqrt{4}} \left( \sqrt{1 - F(3)^2} |0\rangle + F(3) |1\rangle \right) \otimes |3\rangle. \end{aligned}$$

Now, if we operate  $\hat{H}$  on the input qubits, the states are changed to

$$\begin{aligned} \hat{H}|0\rangle &= \frac{|0\rangle + |1\rangle + |2\rangle + |3\rangle}{\sqrt{4}}, \quad \hat{H}|1\rangle = \frac{|0\rangle - |1\rangle + |2\rangle - |3\rangle}{\sqrt{4}} \\ \hat{H}|2\rangle &= \frac{|0\rangle + |1\rangle - |2\rangle - |3\rangle}{\sqrt{4}}, \quad \hat{H}|3\rangle = \frac{|0\rangle - |1\rangle - |2\rangle + |3\rangle}{\sqrt{4}}. \end{aligned}$$

All states are distributed to  $|0\rangle$  with  $+\frac{1}{\sqrt{4}}$  amplitude, hence

$$\begin{aligned} |\psi_0\rangle' &= (\hat{I} \otimes \hat{H}) |\psi_0\rangle \\ &= \left( \frac{F(0) + F(1) + F(2) + F(3)}{4} \right) |1\rangle \otimes |0\rangle + \dots \\ &= f |1\rangle \otimes |0\rangle + \dots \end{aligned}$$

Note that the amplitude of  $|1\rangle \otimes |0\rangle$  is equal to  $f$ . This  $|\psi_0\rangle'$  state thus can be regarded as a quantum coin. We use  $|\psi_0\rangle'$  to perform a rough estimate of  $f$  within  $\delta$  error using  $O(1/\delta^2)$  queries just like Monte Carlo integration. Suppose that the estimated value is  $f_0$ , then we can say that the correct value  $f$  is in the interval  $[f_0 - \frac{\delta}{2}, f_0 + \frac{\delta}{2}]$  with a certain high probability (1st process in Figure 4).

---

**Algorithm 1** Our implementation of QCoin ( $F, k, L$ )

---

```
// 1st step
 $f_0 \leftarrow 0$ 
for  $i = 1$  to  $L$  do
  make QCoin :  $\hat{Q}_{\sqrt{F},0} |0\rangle |0\rangle$ 
  if Measure(QCoin) ==  $|1\rangle$  then
     $f_0 += 1$ 
  end if
end for
 $f_0 /= L$ 

// The other steps
 $E_- \leftarrow 0.0, E_+ \leftarrow 1.0$ 
for  $i = 1$  to  $k$  do
   $\delta \leftarrow \sin(\pi/2^{i+1})$  // hypothetical error
   $E_- \leftarrow \text{Max}(f_{i-1} - \frac{\delta}{2}, E_-)$  // lower bound of error range
   $E_+ \leftarrow \text{Min}(f_{i-1} + \frac{\delta}{2}, E_+)$  // upper bound
   $f_i \leftarrow 0$ 
  for  $j = 1$  to  $L$  do
    make QCoin :  $\hat{G}_{F,E_-}^{2^{i-1}} |0\rangle |0\rangle$ 
    if Measure(QCoin) ==  $|1\rangle$  then
       $f_i += 1$ 
    end if
  end for
   $f_i /= L$ 
   $f_i \leftarrow \text{Min}\left(E_- + \sin\left(\frac{\text{asin}(f_i)}{2^i}\right), E_+\right)$ 
end for

// Output
print  $f_k$ 
```

---

For the next step, we set  $E \equiv f_0 - \frac{\delta}{2}$  and the oracle gate as  $\hat{Q}_{F,E}$ . We make the quantum coin  $|\psi_1\rangle'$  using  $\hat{Q}_{F,E}$  as above:

$$|\psi_1\rangle' = (f - E)|1\rangle \otimes |0\rangle + \dots \quad (32)$$

Now, the amplitude of the target state  $|1\rangle \otimes |0\rangle$  is  $f - E$ . This value is in the interval  $[0, \delta]$ . If we define  $\sin \theta \equiv f - E$ ,

$$|\psi_1\rangle' \equiv \sin \theta |1\rangle \otimes |0\rangle + \dots \quad (33)$$

We then operate AA for  $O(1/\delta)$  times to make the error range from  $[0, \delta]$  to  $[0, 1 - \epsilon]$  (upper limit is not always precisely 1). It can be done without knowing the exact value of  $f$ . If we conduct  $m$  times AA operations, the state is changed as:

$$|\psi_1\rangle'' = \sin(2m + 1)\theta |1\rangle \otimes |0\rangle + \dots \quad (34)$$

This corresponds to the 2nd process in Figure 4. Now, we can estimate the value of  $\sin(2m + 1)\theta$  within  $\delta$  error measuring the state for  $O(1/\delta^2)$  times (3rd process in Figure 4).

We assume the estimated value is  $f_1$ . Then, we can easily calculate back to the original scale: calculate the value of  $\theta$  from  $m$  and  $\sin(2m + 1)\theta$  values, and  $f$  is calculated by the relation " $f = \sin \theta + E$ ". As a result, we get to estimate  $f$  value with the error range  $\delta^2$  (the 4th process in Figure 4). If this step is repeated for  $k$  times, we achieve the error  $\delta^{k+1}$ .

**Convergence rate.** In the case of  $k = 1$  step as above, the estimation error is  $\delta^2$ , and the total number of queries is calculated as:

$$O(1/\delta^2) + (1 + 2O(1/\delta)) \times O(1/\delta^2) = O(1/\delta^3) \quad (35)$$

The convergence rate is improved from " $\delta$  error with  $O(1/\delta^2)$  queries" to " $\delta^2$  error with  $O(1/\delta^3)$  queries". For comparison, assuming the numbers of queries are both  $N$ , the estimation error is reduced from  $O\left(\frac{1}{N^{0.5}}\right)$  to  $O\left(\frac{1}{N^{0.66\dots}}\right)$ .

As for the case of  $k \gg 1$ , we show the convergence rate here. If we use  $M$  queries in the Monte Carlo integration part of QCoin, we achieve  $O(1/\sqrt{M})$  as the error value of  $\delta$  (equivalently,  $\delta = O(1/\sqrt{M})$ ). For a total of  $k - 1$  iterations, QCoin achieves the final error value  $O(\delta^k)$  as described above. On the other hand, the total number of queries  $N$  in this case is asymptotically defined as

$$N = M \cdot O\left(1 + M^{1/2} + \dots + M^{(k-1)/2}\right) = O\left(M^{k/2}\right) \quad (36)$$

for a large enough  $k$ . Given that we have  $\delta = O(1/\sqrt{M})$ , we can conclude that QCoin achieves the final error value of  $O(\delta^k) = O(1/\sqrt{M}^k) = O(1/N)$  using  $N$  queries using QCoin.

**Our contributions over Abrams and Williams.** Compared to the original work by Abrams and Williams [AW99], our work provides the following contributions.

- We conducted numerical experiments to clarify the followings:
  - Abrams and Williams showed only that the convergence rate of QCoin converges to  $O(1/N)$  as  $k$  tends to infinity. We show how this convergence rate varies for a finite (practical)  $k$ .
  - Similar to classical Monte Carlo integration, there is a non-zero possibility that  $f$  resides outside the estimated interval at each step. Its influence to the final outcome is difficult to investigate just by looking at the theory, which we have shown by numerical experiments.
  - Monte Carlo estimates in QCoin result in  $f^2$  (i.e., the probability of "heads") and we need to take its square-root, making its estimation more error-prone toward  $f \approx 0$ . Abrams and Williams did not discuss the consequence of this behavior.
- We redesigned and implemented the whole algorithm of QCoin, as shown in Algorithm 1. Some technical points we implemented are as follows:
  - We show how to deal with the cases where Monte Carlo estimation at each step is outside the range  $[0, 1]$  which has been ignored so far, yet certainly happens in practice.
  - We propose to directly estimate  $f$  for the first estimate using a different quantum coin than the rest.
  - We fix the number of the scaling-shifting operation per step.
- We demonstrated the superiority of QCoin against QSS, for the first time, on an actual quantum computer.
  - We point out that QCoin belongs to a class of hybrid quantum-classical algorithms [KMT\*17] and demonstrate its usefulness on actual quantum computers in the presence of noise (shown and discussed later).

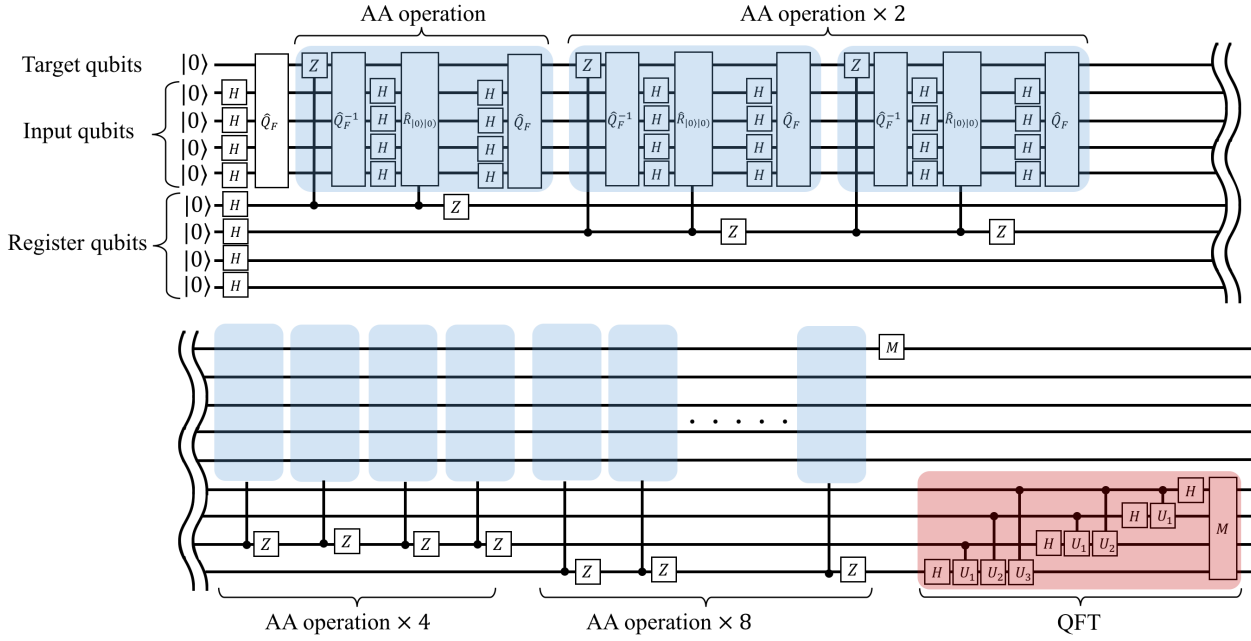


**Figure 5:** Example of the quantum circuit of QSS with 4 input qubits and 4 register qubits case. ( $X, Z$ : Pauli gates,  $\hat{H}$ : Hadamard gate,  $\hat{Q}_F$  and  $\hat{Q}_F^{-1}$ : oracle gate and inverse oracle gate,  $M$ : measurement gate,  $R_{|0\rangle|0\rangle}$ : phase flip gate only for the state  $|0\rangle|0\rangle$ ,  $U_n (n = 1, 2, 3)$ :  $e^{i\frac{\pi}{2^n}}$  phase shift gate for  $|1\rangle$  state.)

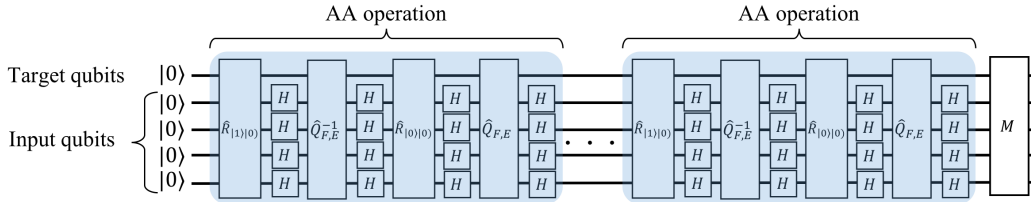


**Figure 6:** Example of the quantum circuit of QCoin with 4 input qubits. ( $\hat{Q}_{F,E}$  and  $\hat{Q}_{F,E}^{-1}$ : oracle gate and its inverse,  $R_{|0\rangle|0\rangle}$  and  $R_{|1\rangle|0\rangle}$ : phase flip gate only for the state  $|0\rangle|0\rangle$  and  $|1\rangle|0\rangle$  respectively.)

## 5. On a Simulator

We now explain our implementations of QSS and QCoin on a simulator of quantum computing using Microsoft Q# [SO18].

**QSS.** The AA operation  $\hat{G}_F$  using from Equation 23 to Equation 24 in QSS is defined as Equation 13:

$$\hat{G}_F \equiv (2|\psi_0\rangle\langle\psi_0| - \hat{I})\hat{Z}. \quad (37)$$

$|\psi_0\rangle$  can be decomposed as Equation 20:

$$|\psi_0\rangle = \hat{Q}_F(\hat{I} \otimes \hat{H})|0\rangle|0\rangle \quad (38)$$

$$\langle\psi_0| = \langle 0| \langle 0| (\hat{H} \otimes \hat{I}) \hat{Q}_F^{-1}. \quad (39)$$

We substitute Equation 38 and 39 to Equation 37, and then we derive the below formulation:

$$\begin{aligned} \hat{G}_F &= \hat{Q}_F(\hat{I} \otimes \hat{H}) (2|0\rangle|0\rangle\langle 0| \langle 0| - \hat{I}) (\hat{I} \otimes \hat{H})^{-1} \hat{Q}_F^{-1} \hat{Z} \\ &= -\hat{Q}_F(\hat{I} \otimes \hat{H}) (\hat{I} - 2|0\rangle|0\rangle\langle 0| \langle 0|) (\hat{H} \otimes \hat{I}) \hat{Q}_F^{-1} \hat{Z}, \end{aligned}$$

where we omit irrelevant register qubits here. If  $(\hat{I} - 2|0\rangle|0\rangle\langle 0| \langle 0|)$  is defined to be represented by  $\hat{R}_{|0\rangle|0\rangle}$ , we have

$$\hat{G}_F = -\hat{Q}_F(\hat{I} \otimes \hat{H}) \hat{R}_{|0\rangle|0\rangle} (\hat{I} \otimes \hat{H}) \hat{Q}_F^{-1} \hat{Z}. \quad (40)$$

The quantum circuit using such AA operation  $\hat{G}_F$  is shown in Figure 5. Each blue-colored region of the circuit corresponds to Equation 40. The operators in Equation 40 are lined up in the reverse order in the circuit (operators are like matrix operations, hence they are indeed conducted from the back of an equation). AA operations are controlled by register qubits, which allows us to store the history of the rotating state vector; only if a control-register qubit is  $|1\rangle$ ,  $\hat{G}_F$  is run and the state vector rotates. Finally, the red region of the circuit performs QFT, which operates on the register qubits and extracts the period.

**QCoin.** The quantum circuit is described in Figure 6. The exact operator  $\hat{G}_{F,E}$  of AA for QCoin  $|\psi_1\rangle'$  in Equation 33 is defined as



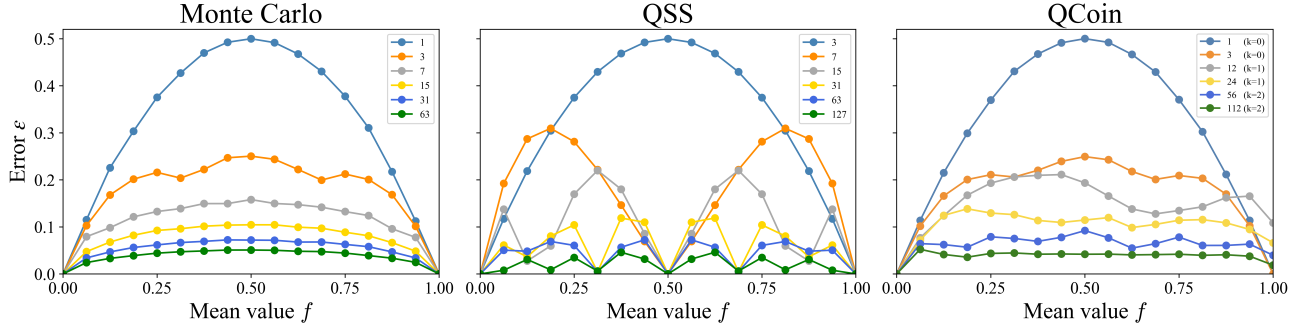


**Figure 7:** Error plots against query times (represented by colors indicated in the legends) with a various target mean  $f$  in three methods; Monte Carlo, QSS, and QCoin.

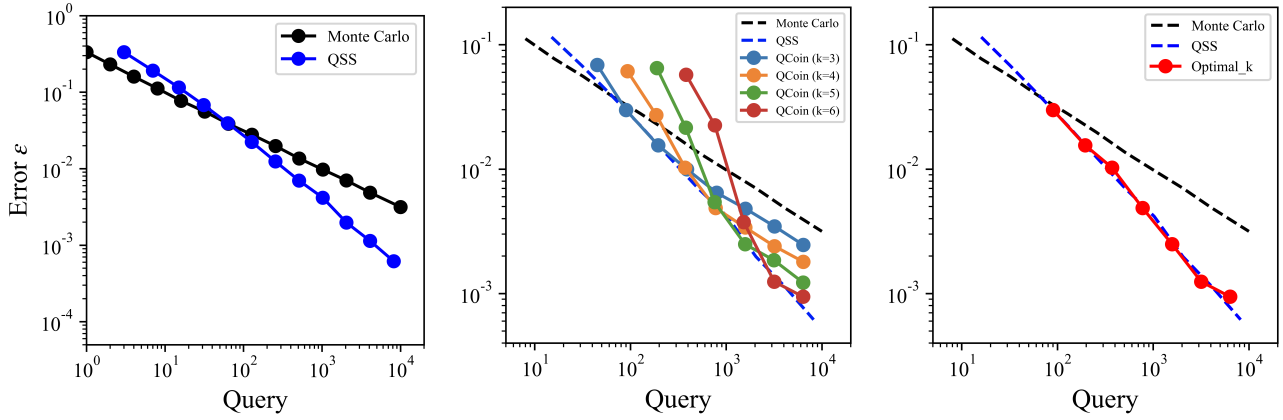


**Figure 8:** (Left and Center) Mean absolute error plots with query times in Monte Carlo, QSS, and QCoin( $k = 3, 4, 5, 6$ ). (Right) The best performance of QCoin with selected optimal  $k$  values is plotted.

the equation 13:

$$\hat{G}_{F,E} \equiv (2|\psi_1\rangle\langle\psi_1| - \hat{I})\hat{R}_{|1\rangle|0\rangle}, \quad (41)$$

where operator  $\hat{R}_{|1\rangle|0\rangle}$  flips the amplitude of  $|1\rangle|0\rangle$ .  $|\psi_1\rangle'$  is decomposed by  $|\psi_1\rangle$  and some gate operations like Equation 31:

$$\begin{aligned} \hat{G}_{F,E} &= (\hat{I} \otimes \hat{H})(2|\psi_1\rangle\langle\psi_1| - \hat{I})(\hat{I} \otimes \hat{H})^{-1}\hat{R}_{|1\rangle|0\rangle} \\ &= (\hat{I} \otimes \hat{H})(2|\psi_1\rangle\langle\psi_1| - \hat{I})(\hat{H} \otimes \hat{I})\hat{R}_{|1\rangle|0\rangle} \end{aligned} \quad (42)$$

and  $|\psi_1\rangle$  is also deconstructed from Equation 30:

$$\begin{aligned} 2|\psi_1\rangle\langle\psi_1| - \hat{I} &= \hat{Q}_{\hat{F},E}(\hat{I} \otimes \hat{H})(2|0\rangle|0\rangle\langle 0| \langle 0| - \hat{I})(\hat{H} \otimes \hat{I})\hat{Q}_{\hat{F},E}^{-1} \\ &= \hat{Q}_{\hat{F},E}(\hat{I} \otimes \hat{H})\hat{R}_{|0\rangle|0\rangle}(\hat{H} \otimes \hat{I})\hat{Q}_{\hat{F},E}^{-1}, \end{aligned} \quad (43)$$

where  $(2|0\rangle|0\rangle\langle 0| \langle 0| - \hat{I})$  is represented by  $\hat{R}_{|0\rangle|0\rangle}$  for simplicity. Substituting Equation 43 to 42, we get the explicit form of  $\hat{G}_{F,E}$ :

$$\hat{G}_{F,E} = (\hat{I} \otimes \hat{H})\hat{Q}_{\hat{F},E}(\hat{I} \otimes \hat{H})\hat{R}_{|0\rangle|0\rangle}(\hat{H} \otimes \hat{I})\hat{Q}_{\hat{F},E}^{-1}(\hat{H} \otimes \hat{I})\hat{R}_{|1\rangle|0\rangle}. \quad (44)$$

## 5.1. Results

Figure 7 shows the behaviors of estimation error against the increasing number of queries with different target mean-values  $f$  in three methods: Monte Carlo, QSS, and QCoin. We conducted numerical experiments with 3000 samples for each point in Monte Carlo and QCoin, and calculated its theoretical error for QSS. In Monte Carlo, all the reduction rates of errors are almost uniform regardless of  $f$ , while QSS returns almost zero error at specific  $f$ . Johnston also showed this distinctively different behavior, which arises from QFT. Fourier transformation extracts a period of data series; therefore, it can detect the frequency of wave whose period matches the data length. In QCoin, however, we see a nearly uniform reduction of error just like Monte Carlo integration. One minor difference occurs at  $f = 1$ , where QCoin has non-zero error while Monte Carlo integration has zero error. This difference arises from the fact that the QCoin algorithm scales the bounded-error of quantum coin  $[0, \delta]$  to  $[0, a]$  ( $a$  is not always 1). If  $a$  is always 1, the QCoin with  $f = 1.0$  only returns  $|1\rangle$  at any steps.

Figure 8 shows the mean error of QCoin with random  $f$  samplings for each  $k$  step. Figure 8 (Left) plots the results of Monte Carlo and QSS. Monte Carlo integration took 10000 samples ( $f$  is

randomly selected for each sample) for each point, and calculate the theoretical error of QSS with uniformly selected 200  $f$  values for each point. In Monte Carlo, the slope of the curve is  $-0.50$  in the logarithmic scale which matches the theoretical convergence rate of  $O(1/\sqrt{N})$  with  $O(N)$  queries. In QSS, the slope is  $-0.85$ ; hence, it achieves  $O(1/N^{0.85})$  error with  $O(N)$  queries. This result is close to the theoretical rate of  $O(1/N)$ .

Figure 8 (Center) shows the results of QCoin with  $k = 3, 4, 5, 6$  cases. For all the  $k$  values, the error of few queries is large because the number of trials of a quantum coin in each step becomes too small for the estimation value to be reasonably accurate for the succeeding shifting-scaling operations. Other than that, the slope for the same  $k$  value first quickly becomes close to  $-1.0$ , but asymptotically approaches to  $-0.5$  after many queries while fixing  $k$ . We can thus observe that there is an optimal number of shifting and scaling operations  $k$  for a given total number of queries.

Figure 8 (Right) plots the results of QCoin with the those optimal  $k$  values for each number of queries. This optimal  $k$  results in almost the same performance as QSS, and we use this optimal  $k$  for the remaining experiments.

Table 1

	Monte Carlo	QCoin on simulator	QCoin on quantum computer
0.0 (black)	0.000	0.000	0.018
0.5 (gray)	0.026	0.014	0.015
1.0 (white)	0.000	0.006	0.011

*Mean absolute error of supersampling images in Figure 1 for each target pixel color (black, gray, and white;  $f = 0.0, 0.5, 1.0$ ) in three methods; Monte Carlo, QCoin on simulator, and QCoin on quantum compute.*

We applied our QCoin method to supersampling an image. For the target, we prepare a boolean image with higher resolution. Figure 1 shows images with ground truth, Monte Carlo, QCoin on a simulator, and QCoin on a real quantum computer, and QSS on a real quantum computer which we discuss more in the next section. Table 1 shows the mean absolute errors. We adopt the same number of queries (240) for Monte Carlo and QCoin. Both Monte Carlo and QCoin return the correct value for 0.0 (black pixels). For 0.5 (gray pixels), QCoin exhibits a better performance than Monte Carlo as the numerical experiments show. The reduction of noise in gray pixels is visible, and the mean error value decreases from 0.026 to 0.014. However, in case of a white pixel, QCoin shows a little error (the mean error is 0.006), while no error occurs in Monte Carlo integration.

## 6. On an Actual Quantum Computer

We use IBM Q5 Yorktown [IBM] and Qiskit [AO19] to run QSS and QCoin on an actual quantum computer. Due to the hardware limitations, we needed to simplify settings for both QSS and QCoin.

**QSS.** To implement QSS, we removed the circuit for input qubits and assumed that the oracle  $\hat{Q}_F$  operates as:

$$\hat{Q}_F |0\rangle = \sqrt{1-f} |0\rangle + \sqrt{f} |1\rangle.$$

The AA operation  $\hat{G}$  is expressed as

$$\begin{aligned} \hat{G} &= \hat{Q}_F (2|0\rangle\langle 0| - \hat{1}) \hat{Q}_F^{-1} \hat{R}_f \\ &= \hat{Q}_F \hat{Z} \hat{Q}_F^{-1} \hat{Z}. \end{aligned} \quad (45)$$

In one qubit case, the  $R_f$  flip gate counterparts to a Pauli Z gate, and the  $(2|0\rangle\langle 0| - \hat{1})$  flip operation also does to  $\hat{Z}$  gate. Despite its very simple implementation, we can create at most 3 qubits circuit (expressed in Figure 9) on the IBM Q5 quantum computer due to its requirement for the architecture of qubits as discussed in the previous section.

**QCoin.** In QCoin, we also simplified the quantum circuit by eliminating the circuit for input qubits and set the oracle as:

$$\hat{Q}_{F,E} |0\rangle = \sqrt{1-f^2} |0\rangle + f |1\rangle.$$

In this case, the oracle can be regarded as the one including the process of making a quantum coin. AA operation  $\hat{G}$  is almost the same as QSS:

$$\begin{aligned} \hat{G} &= \hat{Q}_{F,E} (2|0\rangle\langle 0| - \hat{1}) \hat{Q}_{F,E}^{-1} \hat{R}_f \\ &= \hat{Q}_{F,E} \hat{Z} \hat{Q}_{F,E}^{-1} \hat{Z}. \end{aligned} \quad (46)$$

The quantum circuit is shown in Figure 9.

## 6.1. Results

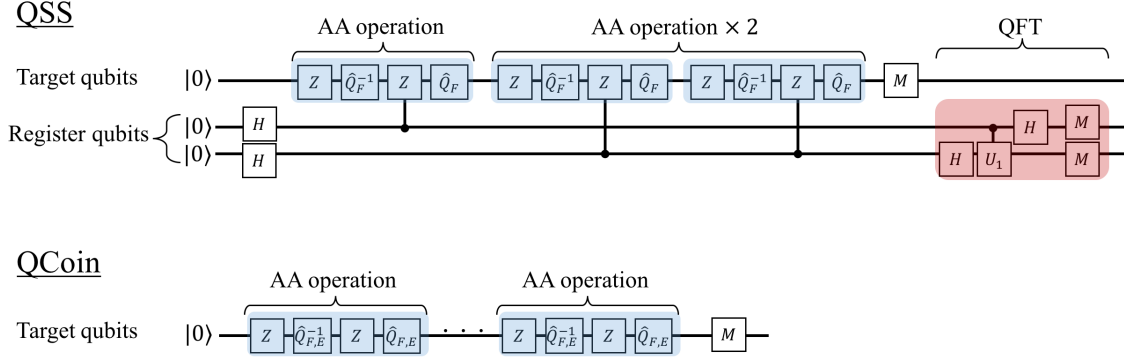
**QCoin.** Figure 10 shows the error of QCoin on the quantum computer with  $f = 0.50$ . All the data points are calculated by 300 simulations. Figure 10 (left) shows the results of Monte Carlo integration and QCoin of  $k = 0$  (equivalent to Monte Carlo integration) on the quantum computer. The convergence rate is almost the same at small numbers of queries ( $\lesssim 100$ ), while the reduction of error stops afterward. We speculate that this error arises from the readout error of qubits which we cannot improve by more trials.

QCoin can overcome this limitation by using the AA steps. QCoin can scale-up the bounded error and measure the scaled quantum coin in each step, as shown in Algorithm 1. We only need a rough estimate of  $f$  for each step; hence, there is less influence of readout error.

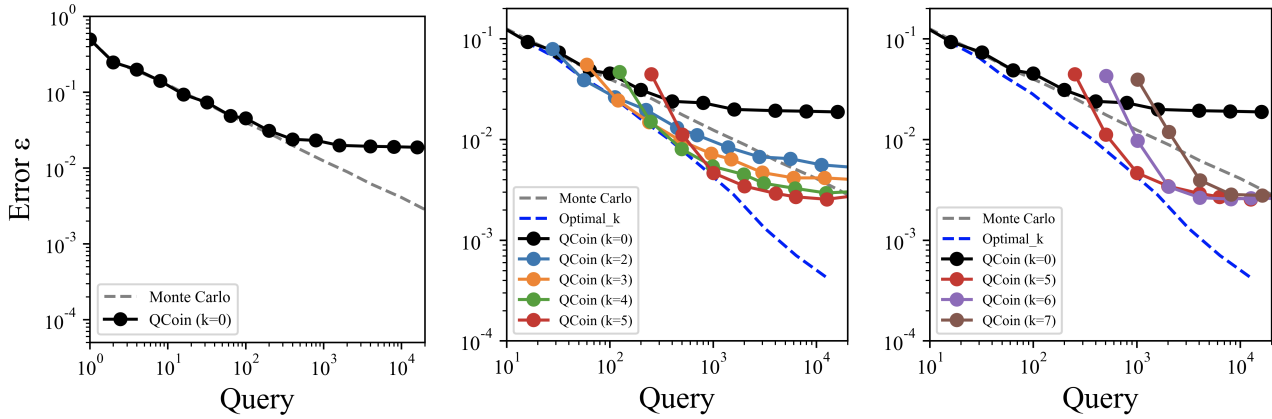
Figure 10 (center) shows  $k = 2, 3, 4, 5$  cases of QCoin. We can confirm that QCoin performs better than Monte Carlo and it is compatible with the results on a simulator when the number of queries is small. QCoin, however, stops converging for a larger number of queries. We speculate that it is due to the readout error, as noted above.

Figure 10 (right) shows the plots of  $k = 6, 7$  cases. The error does not reduce with  $k = 6, 7$  compared to  $k = 5$ , even though QCoin performed more AA steps. We thus think that having more than 16 AA steps (corresponds to the  $k = 5$  case) is meaningless due to the accumulation of decoherence and gate errors in a large quantum circuit.

Given those results, we now come back to the experiment of supersampling shown in Figure 1 and Table 1. For gray pixels, the mean error on an actual quantum computer is almost the same as in simulation. However, the results are sometimes worse for white or black pixels.



**Figure 9:** (Top) QSS’s quantum circuit for 7 queries in minimum setting; no input qubit and two register qubits. (Bottom) QCoin’s quantum circuit in minimum setting; no input qubit.



**Figure 10:** Results of QCoin with  $f = 0.50$  on an actual quantum computer. We plot  $k = 0$  on the left, additionally  $k = 2, 3, 4, 5$  in the center, and  $k = 5, 6, 7$  on the right. Monte Carlo plot data points are calculated with 3000 samples, and Optimal\_k data is plotted with the data points calculated by 500 samples on the simulator.

For white pixels ( $f = 1.0$ ), we infer that decoherence of a qubit causes this error. The dominant process of single-qubit decoherence is the energy relaxation of qubit states from the high-energy state  $|1\rangle$  to the ground state  $|0\rangle$ . Hence, the larger  $f$  becomes, the larger the influence of single-qubit decoherence.

For black pixels  $f = 0.0$ , the error is not coming from quantum decoherence, but from a calculation process as we also observed in the simulation. When  $f$  is very small, the square-root of  $f^2 \rightarrow f$  enlarges the error. On a noiseless simulator, this case arises for  $f = 0.0625$  as shown in Figure 7, which exhibits slightly slower convergence compared to the other cases for 112 queries.

We also show a supersampled-image via QSS in Figure 1. The noise in actual quantum computers significantly influences the computation on almost all the pixels (also observed by Johnston [Joh16]). The mean absolute error becomes 0.30, even though no error should occur for some  $f$  values such as 0.5 according to the simulation. We hypothesize that the domain type of error is multi-

qubit gate error. Multi-qubit operations are more challenging to execute than single-qubit ones because they must support the controlled gates. IBMQ publicly discloses all the gate errors [IBM], and the multi-qubit gate errors are approximately 5%. Therefore, even if we operate it for only a few times, the error accumulates rapidly to the level that is problematic for further computation. QCoin does not suffer from this issue due to its simple circuit and the hybrid nature of classical-quantum algorithms. We thus observe a striking difference between QSS and QCoin when we run both on an actual quantum computer.

## 7. Discussions

**Ray tracing oracle gate.** One might argue that our numerical experiment (inspired by Johnston [Joh16]) is too simple compared to the actual use cases of ray tracing, and then argue that it does not represent the applicability of QCoin in rendering. While we admit that our experiment is not as complex as the actual use cases, the

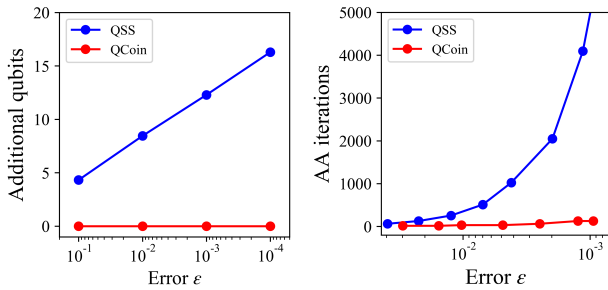


**Figure 11:** The numbers of additional register qubits and AA iterations plotted against the error  $\epsilon$ . QCoin requires a fewer register qubits and less AA iterations to achieve the same error compared to QSS.

basic idea of QCoin is readily applicable to arbitrary complex integrands, just like how Monte Carlo integration is designed. We think that the remaining challenge is to design an oracle gate which efficiently performs ray tracing. While it is theoretically possible to design such an oracle gate, we found it infeasible to perform any numerical experiment (even on a simulator) at this moment for two reasons.

First, the maximum number of qubits we can have at the moment is about 50 qubits [PO18]. It is incorrect to assume that we can get away from this limitation on a simulator. Simulation of 50 qubits already takes roughly 16 peta byte of RAM if we store the full quantum states, and a 64 qubits simulator (on a cluster of 128 nodes) is possible only by limiting the complexity of quantum circuits [CZX\*18]. Given that even *one* floating-point number consumes 32 bits, we concluded that it is currently infeasible to conduct any numerical experiment (both on actual and simulated quantum computers). Note that operations such as the square-root adds up to the required number of qubits. While we should be able to design such a quantum circuit in theory, if we were to perform numerical experiments, even for *simple* cases like ray tracing of a sphere, we need either better hardware or a simulator, which are both out of the scope in this paper.

Second, there is currently no research done on how to *appropriately* represent typical data for ray tracing. For example, due to the limited number of input qubits, it will not be immediately possible to handle triangle meshes on a quantum computer. While Lanzagorta and Uhlmann [LU05] mentioned a theoretical possibility of using Grover’s method for ray tracing, implementation of this idea for any practical scene configurations is currently impossible. We thus believe that further research on a suitable data representation for rendering on quantum computers is deemed necessary, and this topic alone can lead to a series of many research questions and thus cannot be a short addendum in our paper. We focused on a numerical integration algorithm which serves as a building block for ray tracing on quantum computers. Our work should be useful as a stepping stone to conducting further research along this line.

**Error distribution over the image** Rendering is a unique problem of solving many integrals on the image plane, which highlights another difference between QSS and QCoin. In QCoin, the distri-

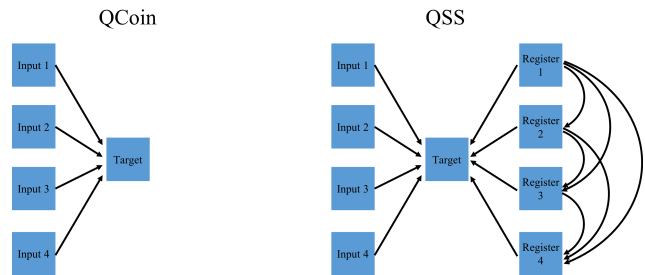


**Figure 12:** Minimum qubits’ architectures for the quantum circuits in Figure 6 (QCoin) and Figure 5 (QSS). The arrow represents a connection with controlled gate; a root qubit at the arrow is a control qubit, and an end-qubit is a target.

bution of errors over the image is essentially noise due to random sampling, which is the same as Monte Carlo integration. Being a hybrid quantum-classical method as we explain later, one can easily apply many existing tools developed for Monte Carlo integration, such as denoising via image-space filtering [ZJL\*15], to QCoin. QCoin can thus directly replace Monte Carlo integration while being asymptotically faster. In QSS, however, erroneous pixels appear as completely wrong pixel values [Joh16] which cannot be easily recovered or identified by the existing tools for Monte Carlo integration. For example, denoising for Monte Carlo rendering would not work as-is for rendered images via QSS. We thus believe that QCoin is more readily applicable to rendering than QSS.

**Required number of qubits.** Quantum computers at this moment have a limited number of usable qubits. As mentioned above, the maximum number of qubits we can have is  $\sim 50$  qubits [PO18] at the moment. Let us consider that the size of the input is  $N$ , and the maximum number of AA iterations is  $P$ . In this case, QSS needs  $\log N + \log P$  qubits to run the algorithm, while QCoin needs only  $\log N$  (left in Figure 11). The examples of quantum circuits for QSS and QCoin also verify this fact (Figure 5 and Figure 6). For example, when the input  $N = 2^{10} = 1024$  is given, using the current architecture of quantum computers, the number of AA iterations in QSS is limited to less than only  $P = 2^5 = 32$  times, whereas QCoin can have no such limitation by construction. This requirement of the number of qubits severely limits the applicability of QSS, making QCoin an attractive alternative in practice.

**Connections among qubits.** Another well-known limitation of quantum computer architecture is the number of connections among qubits. In many quantum algorithms, controlled-gates are important. However, it is currently difficult to prepare all interacting the qubits. For example, IBM Q20 Tokyo [IBM] has a total of 20 qubits, while the size of fully-connected qubits set is only up to 4.

Due to the use of QFT, QSS needs a sequence of qubits which has a connection between the target and the other qubits and full connections among the register (used for computation) qubits. On the other hand, QCoin needs connections only between target and input qubits. Figure 12 shows the minimum qubits’ architectures

(connections) for the quantum circuits in Figure 5 and Figure 6. In general, we need not only more qubits, but also more connections among qubits for QSS than QCoin, which further prevents the use of QSS in real quantum computers.

**Quantum error correction and NISQs.** Aside from errors due to the algorithm (i.e., noise due to a limited number of samples or iterations), the error in quantum computation arises from various factors such as bit-flip errors, decoherence of superposition states, and logic-gate errors. Note that simulators currently do not include such errors. While it is theoretically possible to perform error corrections [KLV00], its implementation on current quantum computers is still considered challenging [RDN\*12]. It is thus generally assumed that one cannot perform calculation accurately as the scale of a quantum circuit (computation time, the number of qubits, and the number of gate operations) is becoming larger.

Such an "unscalable" quantum computer is called an "NISQ" (Noisy Intermediate-Scale Quantum Computer) [Pre18]. On NISQs, quantum algorithms which require many qubits and long computation time will not work due to the errors in actual quantum computers. However, NISQs are more realistic models for actual quantum computers in the near future. Therefore, researchers have been vigorously investigating a novel class of quantum algorithm called "hybrid quantum-classical" [KMT\*17]. In this class of algorithms, an algorithm alternately repeats quantum calculations in a small circuit and adjusting parameters of the quantum circuit based on the classical calculation. A hybrid quantum-classical algorithm generally needs fewer qubits and lower depth of quantum circuit, thus suitable to run on NISQs.

Figure 11 (right) shows the relationship between the number of AA iterations and the estimation error appear for QSS. One can observe that QSS requires more AA iterations and a larger circuit for one continuous quantum operation than for QCoin does. In our experiment and the experiment by Johnston [Joh16], QSS does not perform well on NISQs. Based on its performance on a simulator, we hypothesize that its inferior performance on an actual quantum computer is not owing to the limited number of AA iterations, but its use of many qubits and controlled-gate operations. We should also mention that we could not run a large enough quantum circuit for QSS due to the restriction of the qubit architecture to fully confirm the influence of decoherence alone.

On the other hand, our QCoin method performs well on an actual quantum computer. It is because QCoin is hybrid quantum-classical; the use of a quantum coin is done as in classic Monte Carlo integration while shifting and scaling of the error interval are done by AA in quantum computation. Hybrid quantum-classical algorithms generally need fewer qubits and lower depth of the quantum circuit, which is considered suitable to run on NISQs. While the idea of QCoin was invented a while ago [AW99], there has been no effort to investigate whether QCoin is executable on NISQs, and we think that this finding alone is worthwhile to mention.

## 8. Limitations

Aside from the limited complexity of integrands due to the current architecture of quantum computers, we have a few more

limitations. In classic computers, by giving up the use of random numbers, it is possible to perform quasi-Monte Carlo integration [MC95] to achieve the convergence rate of  $O(\log(N)^s/N)$  for  $s$ -dimension integrands. While the QCoin's convergence rate of  $O(1/N)$  is still better, it is unclear if and how we can incorporate quasi-Monte Carlo to achieve an even better convergence rate. The classical part of QCoin is thus still limited to Monte Carlo. Moreover, due to the constraints of hardware, our experiments for both QSS and QCoin on an actual quantum computer omitted the input circuit part, which generally involves controlled-gate operations. As such, if we could have included the omitted input part, errors in our experiments might potentially go up due to the use of more controlled-gate operations.

## 9. Conclusion

We proposed a concrete algorithm of QCoin and performed numerical experiments for the first time after 20 years of its theoretical introduction [AW99]. Our implementation of QCoin shows a faster convergence rate than that of classical Monte Carlo integration. This performance is equivalent to QSS. We formulated QCoin as a hybrid quantum-classical method and explained why QCoin is more stable than QSS in the presence of noise in actual quantum computers. We discussed hardware limitations of near-term quantum computers and concluded that QCoin needs fewer qubits and simpler architecture, thus being much more practical than QSS. Our experiments on a quantum computer confirmed this robustness against noise and faster convergence rate than classical Monte Carlo integration. We believe that QCoin is a practical alternative to QSS if we were to run rendering algorithms on quantum computers in the future.

**Acknowledgements.** The authors would like to thank Adrien Gruson and Damien Lavoie for their comments on the initial draft.

## References

- [AO19] ALEKSANDROWICZ G., OTHERS: Qiskit: An open-source framework for quantum computing, 2019. doi:10.5281/zenodo.2562110. 10
- [AW99] ABRAMS D. S., WILLIAMS C. P.: Fast quantum algorithms for numerical integrals and stochastic processes. *arXiv* (Aug. 1999). 1, 6, 7, 13
- [BdSGT11] BRASSARD G., DN SEBASTIEN GAMBS F. D., TAPP A.: An optimal quantum algorithm to approximate the mean and its application for approximating the median of a set of points over an arbitrary distance. *arXiv* (June 2011). 4
- [BHT06] BRASSARD G., HÄYER P., TAPP A.: Quantum counting. *International Colloquium on Automata, Languages, and Programming* (May 2006). doi:10.1007/BFb0055105. 4, 5
- [CZX\*18] CHEN Z.-Y., ZHOU Q., XUE C., YANG X., GUO G.-C., GUO G.-P.: 64-qubit quantum circuit simulation. *Science Bulletin* 63, 15 (2018), 964–971. 12
- [DBE95] DEUTSCH D. E., BARENCO A., EKERT A.: Universality in quantum computation. *Proceedings of the Royal Society of London. Series A: Mathematical and Physical Sciences* 449, 1937 (1995), 669–677. 3
- [Gro96] GROVER L. K.: A fast quantum mechanical algorithm for database search. In *STOC '96 Proc. of the twenty-eighth annual ACM symposium on Theory of Computing* (1996). doi:10.1145/237814.237866. 1, 3



- [Gro98] GROVER L. K.: A framework for fast quantum mechanical algorithms. In *STOC '98 Proc. of the thirtieth annual ACM symposium on Theory of computing* (1998). doi:10.1145/276698.276712. 4
- [IBM] IBMQ: Ibmq experience [online]. (web site) <https://quantumexperience.ng.bluemix.net/qx/devices>. 10, 11, 12
- [Joh16] JOHNSTON E. R.: Quantum supersampling. In *Proc. SIGGRAPH Talks '16* (2016). (Presentaiton video at SIGGRAPH 2016) <https://vimeo.com/180284417>. doi:10.1145/2897839.2927422. 1, 4, 5, 11, 12, 13
- [Kaj86] KAJIYA J. T.: The rendering equation. In *ACM SIGGRAPH computer graphics* (1986), vol. 20, ACM, pp. 143–150. 3
- [KLV00] KNILL E., LAFLAMME R., VIOLA L.: Theory of quantum error correction for general noise. *Physical Review Letters* 84, 11 (2000), 2525. 13
- [KMT\*17] KANDALA A., MEZZACAPOI A., TEMME K., TAKITA M., BRINK M., CHOWI J., GAMBETTA J.: Hardware-efficient variational quantum eigensolver for small molecules and quantum magnets. *Nature* 549 (Sept. 2017), 242. doi:10.1038/nature23879. 2, 7, 13
- [KSKAC02] KELEMEN C., SZIRMAY-KALOS L., ANTAL G., CSONKA F.: A simple and robust mutation strategy for the metropolis light transport algorithm. In *Computer Graphics Forum* (2002), vol. 21, Wiley Online Library, pp. 531–540. 3
- [LU05] LANZAGORTA M., UHLMANN J.: Quantum rendering: an introduction to quantum computing, quantum algorithms and their applications to computer graphics. In *SIGGRAPH '05 ACM SIGGRAPH 2005 Courses* (2005). doi:10.1145/1198555.1198722. 1, 12
- [MC95] MOROKOFF W. J., CAFLISCH R. E.: Quasi-monte carlo integration. *Journal of computational physics* 122, 2 (1995), 218–230. 13
- [NC11] NIELSEN M. A., CHUANG I. L.: *Quantum Computation and Quantum Information: 10th Anniversary Edition*. Cambridge University Press, 2011. 2, 3, 4
- [NW99] NAYAK A., WU F.: The quantum query complexity of approximating the median and related statistics. In *STOC '99 Proc. of the thirty-first annual ACM symposium on Theory of computing* (1999). doi:10.1145/301250.301349.
- [Par70] PARK J. L.: The concept of transition in quantum mechanics. *Foundations of Physics* 1 (1970), 23–33. 3
- [PO18] PEDNAULT E., OTHERS: Breaking the 49-qubit barrier in the simulation of quantum circuits. *arXiv* (Dec. 2018). 12
- [Pre18] PRESKILL J.: Quantum computing in the nisq era and beyond. *Quantum* 2 (Aug. 2018), 79. doi:10.22331/q-2018-08-06-79. 13
- [RDN\*12] REED M. D., DICARLO L., NIGG S. E., SUN L., FRUNZIO L., GIRVIN S. M., SCHOELKOPF R. J.: Realization of three-qubit quantum error correction with superconducting circuits. *Nature* 482, 7385 (2012), 382. 13
- [SO18] SVORE K. M., OTHERS: Q#: Enabling scalable quantum computing and development with a high-level dsl. In *Proceedings of the Real World Domain Specific Languages Workshop 2018* (Feb. 2018). doi:10.1145/3183895.3183901. 8
- [TKI99] TOKUNAGA Y., KOBAYASHI H., IMAI H.: Applications of grover's quantum search algorithm. *IPSJ SIG Notes* 70, 5 (Nov. 1999), 33–40. 4
- [ZJL\*15] ZWICKER M., JAROSZ W., LEHTINEN J., MOON B., RAMAMOORTHI R., ROUSSELLE F., SEN P., SOLER C., YOON S.-E.: Recent advances in adaptive sampling and reconstruction for monte carlo rendering. In *Computer Graphics Forum* (2015), vol. 34, Wiley Online Library, pp. 667–681. 12